3D imaging of cell interactions with electrospun PLGA nanofiber membranes for bone regeneration

Urszula Stachewicz[1,2,3], Tuya Qiao[2], Simon C. F. Rawlinson[4], Filipe Viga De Macedo Almeida[2], Wei-Qi Li[2], Michael Cattell[5] and Asa H. Barber[1,2,6]*

[1] Nanoforce Technology Ltd., Queen Mary, University of London, Mile End Road, London E1 4NS, United Kingdom

[2] School of Engineering and Materials Science, Queen Mary, University of London, Mile End Road, London E1 4NS, United Kingdom

E-mail: qiaotuya1227@163.com

E-mail: f.almeida@qmul.ac.uk

E-mail: wei-qi.li@qmul.ac.uk

[3] AGH University of Science and Technology, International Centre of Electron Microscopy for Materials Science and Faculty of Metals Engineering and Industrial Computer Science, Al. A. Mickiewicza 30, 30-059 Kraków, Poland

E-mail: ustachew@agh.edu.pl

[4] Research Centre for Oral Growth and Development, Barts and The London, Queen Mary's School of Medicine and Dentistry, Queen Mary, University of London, 4 Newark Street, London E1 2AT, United Kingdom

E-mail: s.c.f.rawlinson@qmul.ac.uk

[5] Centre for Adult Oral Health, Institute of Dentistry, Barts and The London, Queen Mary's School of Medicine and Dentistry, Queen Mary, University of London, Turner Street, Whitechapel E1 2AD, United Kingdom

E-mail: m.cattell@qmul.ac.uk

[6] School of Engineering, University of Portsmouth, Portsmouth PO1 3DJ, United Kingdom

E-mail: asa.barber@port.ac.uk

Corresponding Author (*) Email: asa.barber@port.ac.uk

Phone: +44 (0)23 9284 2363

Fax: +44 (0)23 9284 3082

Address: University of Portsmouth , Anglesea Building, Anglesea Road, Portsmouth PO1 3DJ UK

Abstract

The interaction between resident cells and electrospun nanofibers is critical in determining resultant osteoblast proliferation and activity in orthopedic tissue scaffolds. The use of techniques to evaluate cell-nanofiber interactions is critical in understanding scaffold function, with visualization promising unparalleled access to spatial information on such interactions. 3D tomography exploiting focused ion beam (FIB)-scanning electron microscopy (SEM) was used to examine electrospun nanofiber scaffolds to understand the features responsible for (osteoblast-like MC3T3-E1 and UMR106) cell behavior and resultant scaffold function. 3D imaging of cell-nanofiber interactions within a range of electrospun poly(D,L-lactide-co-glycolide acid) (PLGA) nanofiber scaffold architectures indicated a coherent interface between osteoblasts and nanofiber surfaces, promoting osteoblast filopodia formation for successful cell growth. Coherent cell-nanofiber interfaces were demonstrated throughout a randomly organized and aligned nanofiber network. Gene expression of UMR106 cells grown on PLGA fibers did not deviate significantly from those grown on plastic, suggesting maintenance of phenotype. However, considerably lower expression of *Ibsp* and *Alpl* on PLGA fibers might indicate that these cells are still in the proliferative phase compared with a more differentiated cell on plastic. This work demonstrates the synergy between designing electrospun tissue scaffolds and providing comprehensive evaluation through high resolution imaging of resultant 3-dimensional cell growth within the scaffold.

Keywords: 3D tomography, FIB-SEM, 3D imaging, electrospinning, nanofibers, PLGA, osteoblast, tissue engineering

1. Introduction

The production of nano- and micro-structured scaffolds for tissue engineering has required concurrent development in imaging techniques to evaluate cell interaction and growth on biomaterials. While the effectiveness of tissue-engineered scaffolds has been reported as being dependent on their mechanical stability [1], chemical composition [2], and biological compatibility [3], the interaction between the scaffold and cells [4] is critical for resultant viability, cell activation [5] and focal adhesion formation [6]. Thus, imaging techniques are often employed to quantify these scaffold-cell interactions through direct visualization. Orthopedics is an important area where tissue engineering exploits biomaterials to promote cell adhesion, but understanding osteoblast behavior and adhesion is required to effectively optimize bone-biomaterial interfaces [7]. Electrospun scaffolds are used widely in regenerative medicine for orthopedic applications due to the high porosity of the 3D spun network that has been shown to promote cell proliferation [8-9] and invasion of host tissue. Thus, the architecture of electrospun scaffolds and their surfaces is advantageous in tissue engineering for shaping and directing cell growth [10]. The fibrous architecture is easily controllable in electrospinning and has been notably varied to increase the pore size and spacing between fibers using low-temperature electrospinning [11] or controlling fiber organization by employing patterned and rotating collectors [12]. Such control of electrospun fiber network architecture allows engineering of cell migration through the scaffolds [13]. Prevalent examples of polymers electrospun into effective tissue scaffolds include polydioxanone [14], poly(ε-caprolactone) [15], polyglycolic acid (PGA) [16], polylactic acid (PLA) [17], poly(L-lactide) [18] and their copolymers poly(D,L-lactide-co-glycolide) (PLGA) [19-23] that are often exploited as high surface area fibrous membranes [24-25]. Electrospinning is particularly notable as the predominant method used to produce synthetic

fibers in the nanometer range to mimic the collagen matrix and is therefore most promising in bone regeneration and cartilage regeneration [17, 26]. Electrospun materials including PLGA have the potential to biomimic the structure of natural bone [19].

Production of electrospun fibers for tissue scaffolds is currently popular due to the ease of selecting processing parameters, particularly to control fiber diameters ranging from 10 nm up to a few microns [27-28]. Further control of the fiber organization into an aligned network has been achieved by deposition of nanofibers onto a rotating drum collector [29-31]. Such a method reduces spacing between fibers and decreases the resultant pore size in the spun membrane comparing to a randomly deposited system. The resultant increase in surface area to volume of electrospun nanofibers in both random and aligned arrangements has a considerable geometric advantage over larger fiber diameters [30]. However, optimization of the electrospinning process and understanding cell growth from their interaction with nanofiber surfaces is yet to be fully determined. Previous work has used PLGA fibers to rebuild the natural 3D environment for enhanced skin cell and tissue growth by imitating the fibrillar structure and ECM, as well as providing the necessary direction for cell function, organization and survival [21]. Many studies have also shown the biocompatibility of PLGA with osteoblasts, highlighting PLGA as a preferred material to promote bone regeneration [19-24]. Bone regeneration is complex [32] and therefore any orthopedic application utilizing PLGA electrospun tissue scaffolds must be evaluated to ensure that normal osteoblast behavior is maintained in the new environment.

Adhesion between osteoblasts and the biomaterial substrate surface is critical in guiding growth and is characterized by focal adhesion contacts and F-actin supported finger-like protrusions of the plasma membrane known as lamellipodia and filopodia [7]. The elongation of these structures facilitates osteoblast migration and adhesion to the extracellular matrix (ECM) in

wound healing [33]. Filopodia regulate cell motility and therefore require understanding of their growth in 3D. Moreover, quantifying filopodia in terms of size, numbers and growth direction are relevant for cell motility studies [34] and assessing the suitability of the manufactured substrate. Evaluation of membranous outgrowths is typically achieved using fluorescence microscopy but is relatively ineffective as some filopodia diameters are of the order of 200 nm, which is below the resolution of many optical techniques. Despite confocal microscopy commonly being employed to view cells in 3D structures, the penetration of light in dense scaffolds is limited to 200 microns [35]. X-ray computed tomography (CT) can be used to image through dense scaffolds to characterize the electrospun fibers but the resolution is limited to microns [11]. Thus, scanning electron microscopy (SEM) has been shown to be highly effective in evaluating sub-micron filopodia development at surfaces in 2D [36]. While SEM is recognized as possessing sufficient (nanometer) resolution to image a range of biomaterial surfaces, recent work has extended SEM by combining focus ion beam (FIB) microscopy to study cell-substrate interfaces at patterned surfaces, cells and ECM [37]. FIB-SEM uses both FIB to section through a material and SEM to image exposed surfaces following the FIB sectioning, which is typically referred to as 'slice-and-view' [38-39]. Collection of 2D SEM images during this sectioning is subsequently reconstructed to provide a 3D image of the interrogated sample. FIB-SEM tomography is widely used in studying microstructure changes in superalloys [40] as well as biological and geological materials [41]. Recently, FIB-SEM has been used to investigate the cell-substrate interaction between microneedle arrays [42] and complex structures including interconnections of dentine tubules [39]. Despite the introduction of FIB-SEM as a high-resolution imaging tool, evaluation of the cellular interactions with porous tissue scaffolds is lacking. Indeed, FIB-SEM is particularly suited to the study of tissue scaffolds with structural

features below the resolution of optical microscopy. Such imaging is applied to PLGA, as a medically approved material, organized into random and aligned nanofiber architectures to investigate 3D cell proliferation across the relatively large scaffold volume as well as at the smaller cell-nanofiber interfaces. This paper therefore attempts to quantify fiber stability and visualize the interaction of osteoblasts with electrospun PLGA fiber networks intended for guided bone regeneration for bone scaffold applications. The interaction between filopodia and the nanofiber membrane is visualized using 3D imaging based on FIB-SEM 'slice-and-view' methods and correlated with confocal microscopy and gene expression. This 3D analysis allows direct investigation of cell proliferation depth into the electrospun membrane and considers the influence of fiber spacing on cell proliferation using aligned and random fibrous organizations.

2. Materials and Methods

2.1. Electrospinning PLGA scaffold

Polymer solutions for electrospinning were prepared using poly(D,L-lactide-co-glycolide acid) (PLGA - lactide:glycolide (75:25), molecular weight: 66,000-107,000, Sigma Aldrich, U.K.) dissolved in a mixture of chloroform (analytical reagent grade, Fischer Scientific, U.K.) and N,N –dimethylformamide (DMF, 99.8 %, Sigma Aldrich, U.K.) (85/15 mass ratio) within a glass vessel to produce a resultant polymer concentration of 15 wt. % in solution. Electrospinning of PLGA was achieved using a single nozzle setup and a voltage of 14-15 kV applied between the nozzle and a ground electrode positioned 20 cm below the spinning nozzle. Polymer solution was supplied with a syringe pump at a flow rate of 0.5 - 1 $\mu l.h^{-1}$. The applied voltage at the metal needle caused charge build-up at the polymer solution meniscus hanging at the end of the nozzle until cone-jet formation and stretching jets towards the ground electrode occurred, resulting in

solid nanofiber deposition on glass microscope slides (25×37 mm) placed on an aluminium foil connected to the ground electrode. Aligned fibers were electrospun with an applied voltage of 20 kV using a distance of 15 cm between the metal needle and a rotating collector. The flow rate at the syringe pump was 1 $\mu l.h^{-1}$ and rotation speed of the drum was 3500 rpm, providing a surface drum velocity of 550 $m.min^{-1}$. The average temperature and humidity during electrospinning was 22.3 °C and 28-36% respectively. All nanofiber samples were deposited onto glass slides attached to the aluminum foil collector. The produced fibers are presented in SEM images shown in Figure 1 with a size distribution histogram. The glass slides were removed from the aluminium foil after electrospinning and edges of the collected fibers secured to the edges of the supporting glass slide substrate using a light body regular set hydrophilic vinyl polysiloxane impression material (Virtual, PL4063, setting time 4 min 30 s, Ivoclar-Vivadent, Lie.) to avoid any fiber mat damage during the cell culturing process.

2.2. Morphological analysis of PLGA fibers

Cell proliferation is expected to be dependent on the organization and geometry of the electrospun fibers. Potential PLGA degradation will therefore cause changes in fiber geometry and requires evaluation. Degradation testing of electrospun PLGA fibers mats was performed in either cell culture medium at 37 °C in a humid atmosphere under 10% CO_2 or dry conditions at room temperature (~22 °C). The electrospun PLGA mats were kept in these environments in darkness for more than 8 weeks. Fiber diameter size distribution analysis was performed using image analysis (ImageJ, NIH, U.S.A.) in order to quantify possible PLGA fiber degradation for all samples. A total of 100 fiber diameter measurements from SEM images of each sample were used to produce the corresponding histograms as shown in Figure 1 in Ref [43].

2.3. Cell Culture on PLGA electrospun substrates

All PLGA samples were sterilized by immersion in 70 % ethanol, air dried in a sterile culture hood and both sample sides exposed to UV for 10 min. prior to cell seeding. 2 ml (450,000 cells per ml) of medium containing either rat osteoblast cell line (UMR 106, ATCC® CRL-1661™) or mouse cell line (MC3T3-E1, subclone 14, ATCC® CRL-2594™) was added to each sample and cultured at 37 °C in a humid atmosphere under 5% CO_2 for 4 days. Cells were cultured using Lonza Bio DMEM medium containing 4.5 g L-glutamine, 2% Fetal Calf Serum (FCS, Sigma–Aldrich, U.K.) for UMR 106 and 10% Fetal Bovine Serum (FBS, Sigma–Aldrich, U.K.) for MC3T3-E1, and penicillin/streptomycin (Invitrogen, U.K.) 100 units.ml^{-1}. Two microscope slides were placed per Petri dish. We kept low seeding density per unit area due to medium dispersion over the whole surface of the microscope slides. The medium was refreshed twice a week. Cells in PLGA nanofiber mats appeared healthy, with no dead cells visually observed in media, during the total culturing time of 4 days.

2.4. Scanning Electron Microscopy and Focus Ion Beam

Sample preparation for 3D imaging was achieved by fixing the non-degraded PLGA nanofiber mat with osteoblasts after 4 days incubation in glutaraldehyde for 2 h and storing at 4 °C. Elimination of water from the sample was achieved by removing the PLGA nanofiber mat with osteoblasts from storage and submerging three times in a series of the water-ethanol solutions with an ethanol concentration and amount of time as follows: 50% - 5 min., 70% - 5 min., 90% - 5 min. and 100% - 5 min. Samples were finally submerged in hexamethyldisilazane (HMDS, Sigma-Aldrich, U.K.) for 1 min. and air-dried. The solvents replaced water in the sample and

were allowed to dry in air at room temperature to achieve sample dehydration. Conventional 2D SEM imaging was carried out on gold coated samples. 3D imaging of the cells seeded within the electrospun PLGA fiber mat was achieved using a dual beam system (Quanta 3D, FEI, E.U./U.S.A.) integrating an SEM with a FIB. The sample stage was tilted so that the sample surface was perpendicular to the FIB direction and 52° incident to the electron beam [44], with examples of SEM images presented in Figures 2-4. Osteoblasts were stained with 1 % uranyl acetate and 4 % osmium tetroxide (Sigma-Aldrich, U.K.), to improve the contrast between cells and fibers prior to SEM imaging. Visualization of the electrospun fibers and cells was achieved by building on previous protocols [44-45]. Specifically, the dual beam system allows both imaging of surfaces with SEM and removal of the surface layer using FIB to allow further SEM imaging. Collection of 2D SEM images as the FIB mills through samples is used for subsequent 3D reconstruction. Before sectioning through the chosen area of the sample, a part of the proceeding material was removed in order to provide an unobstructed view of the material cross-section, as shown in Figure 3 in Ref [43]. Cross-sectional slices of 100 nm in thickness were milled using FIB from the block of the nanofiber sample at 30 kV and a beam current of 0.3 nA in order to remove ion beam artifacts from the sample [46-47]. An example of resultant SEM imaging of an individual osteoblast fixed to the surface of the electrospun PLGA mat that is subsequently sectioned progressively using FIB to expose subsurface information is presented in Figure 2 in Ref [43]. The collected SEM images during FIB sectioning were filtered using Image J (version 1.46r, NIH, U.S.A.) with the electrospun nanofibers and cells artificially colored for reconstruction as shown in Figure 4 and videos 1, 3, 5 and 7 in Ref [43]. The 3D reconstruction of the nanofiber sample was obtained using Resolve RT (Avizo fire, version 5.2– FEI Edition, Ger.), as shown in Figures 5-7 and in videos 2, 4, 6 and 8 in Ref [43]. The volume occupied

analyses of 3D reconstructed sample were performed using color thresholding and the percentage area covered function on individual images using Image J. The collected images from FIB-SEM were sectioned into approximately 1 μm thick slices for the analysis of volume occupied by osteoblasts and electrospun PLGA fibers as a function of z-axis depth as shown in Figures 5 in Ref [43].

2.5. Immunostaining

For immunofluorescence microscopy, cells were fixed for 10 minutes with 4% (w/v) paraformaldehyde (Sigma-Aldrich, U.K.) and permeabilised with 0.2% (v/v) Triton X-100 (Sigma-Aldrich, U.K.) in phosphate-buffered saline (PBS, Sigma-Aldrich, U.K.) for 10 minutes at room temperature. After three washes in PBS, samples were blocked for 1 hour in 10% bovine serum (BioSera, France) containing 0.25% fish gelatin (Sigma-Aldrich, U.K.). Samples were subsequently incubated with mouse anti-paxillin antibody (BD Biosciences, US) overnight at 4 °C, followed by AlexaFluor 555 antiserum (1:1000, Sigma-Aldrich, U.K.), AlexaFluor 455 phalloidin (1:1000, Sigma-Aldrich, U.K.) and DAPI (4,6-diamidino-2-phenylindole, 1:1000, Sigma-Aldrich, U.K.) for 1 hour at room temperature. Anti-paxillin is selected due to effectiveness as a label for dynamic focal adhesion sites associated with migrating cells. Finally, samples were mounted on glass slides with Mowiol reagent (Sigma-Aldrich, U.K.).

That confocal microscopy was used to image the immunostained samples. Confocal microscopy images were acquired with a Leica TCS SP2 laser scanning confocal microscope using a Leica HCX PL APO Lbd.BL 63x/1.4 oil objective. The field of view (238.1 μm × 238.1 μm) was captured into 8-bit file with a pixel format of 1024 × 1024, which in turn created a pixel size of 232.5 nm × 232.5 nm. The Alexa Fluor 455 was excited by the 488 nm line of an argon ion laser and filtered through the 500-550 nm band-pass emission filter. The Alexa Fluor 555 was excited

by the 543 nm line of a Helium/Neon ion laser and filtered through the 560-600 nm band-pass emission filter. The AOBS power and gain value were adjusted below the fluorophore saturation level and then applied for the acquisition of all images. All samples were scanned in x-y-z mode. The interval between sections was set as 0.3 μm and the image stack was displayed as maximum projection in the x-y plane, as presented in Figures 9. The z-stacks were visualized three-dimensionally using Imaris software (Bitplane, version7.7, Swi.). Each channel (i.e. DAPI and F-actin, blue and green, respectively) was reconstructed by performing a smoothed thresholding. The intensity levels were determined by visual inspection (Figures 9).

2.7. Gene expression

2.7.1.RNA extraction

Total RNA from UMR106 osteoblast-like cell line was extracted from three groups of cells cultured for 4 days on random PLGA fibers or tissue culture plastic using an RNeasy Fibrous Tissue Mini Kit (Qiagen, Ger.) as per protocol. Cell coverage on PLGA fiber samples was approximately 6-8 cm^2, whereas cell coverage proceeded over a significantly larger area of 25 cm^2 for the plastic flask control. Subsequently isolated RNA was used as a template for reverse transcriptase to form complementary DNA (cDNA). The expression of selected genes from cDNA samples was performed via quantitative real-time polymerase chain reaction (qRT-PCR).

2.7.2. qRT-PCR analysis

Gene array data was validated by qRT-PCR using TaqMan Assay-On-Demand oligonucleotides for the following genes (Table 1). Each TaqMan assay ran in four replicates. Assays continued with 2 x Absolute qPCR ROX Master Mix (Abgene) on Applied Biosystems 7900 Fast Real-Time PCR System using universal cycling conditions (10 min at 95 °C; 15 s at

95 °C, 1 min 60 °C, 60 cycles). The assays and samples were analyzed on 384 well plates. Data normalization with *Eif4a2* (Eukaryotic initiation factor 4A-II) was chosen as the reference 'housekeeping' gene because the CT values showed the least variation across the samples (Figure 6 in Ref [43]. Each replicate CT was normalized to the average CT of *Eif4a2* by subtracting the average CT of *Eif4a2* from each replicate to give the ΔCT, which is equivalent to the log2 difference between endogenous control and target gene. A raw CT value of 34 represents approximately ten transcript molecules (assuming 100% amplification efficiency). At a copy number less than five, stochastic effects dominate and data generated are less reliable. Thus, a raw CT of 35 was set as the limit of detection in this study and individual replicates that gave CT values >35 were considered not detected. This protocol matches our previous work assessing gene expression on cultured cells using the same equipment and methods of preparation [48-50].

2.7.3. Statistical analysis

The data is presented as a mean of number of sample, n=3 (SD=standard deviation) and analyzed using a Student's T-test with significance level set at $p < 0.050$.

3. Results

3.1 Morphological analysis of PLGA fibers and cell proliferation

PLGA electrospun fiber mats were imaged directly using secondary electron SEM imaging and displayed a regular fibrous structure as shown in Figure 1. The fibers aligned in the direction of the rotating drum exhibited smaller average fiber diameters than for randomly deposited fibers shown in Figure 1. Moreover, the size distribution for the randomly deposited fibers was larger

than for fibers aligned on the rotating drum. SEM imaging of the electrospun fibers in Figures 1 also suggests a smaller spacing for aligned compared to randomly collected fibers.

Degradation of electrospun PLGA is potentially critical in cell proliferation as the geometry of the electrospun mat may change, producing a consequently dynamic structure presented to the osteoblasts. Fiber diameter size distribution analysis was performed in order to quantify potential PLGA fiber degradation as shown in Figure 1(c) and 1(f) in Ref [43]. A slight decrease in the PLGA fiber diameter kept in dry conditions was observed over 2 weeks of the test (Figure 1(a) and 1(b) in Ref [43]), whereas samples kept in cell culture medium increased their diameter, resulting in pore size decreases as observed with SEM progressing from Figure 1(d) and 1(e) in Ref [43]. Large changes in fiber diameter are observed in media conditions. 70% of fiber diameters were below 1 μm after 2 days in medium whereas only 20% fiber diameters are below 1 μm after two weeks in medium. After 4 weeks we obtain similar fiber diameter distributions in wet and dry conditions as after 2 weeks (see Figure 2 in Ref [43]). After more than 8 weeks, the samples porosity was significantly reduced and fiber structures were difficult to identify for the size distribution measurements as shown in Figure 1 (k) in Ref [43].

Secondary electron imaging demonstrated osteoblast adherence to the nanofiber mat surface and within the fibrous membrane after 4 days in culture, as presented in Figure 2. Osteoblast morphology is related to substrate presentation; cells appear more elongated when grown on aligned fibers compared to cells seeded on randomly oriented fibers, as shown in Figures 3, indicating the dominance of the fiber principle axis in directing cell growth. Filopodia localized at the edges of osteoblasts were observed in Figures 4, (indicated with arrows) and promote the sheets of cells to align in the nanofiber direction and participate in cell-cell adhesion.

3.2. 3D reconstruction from FIB-SEM (3D tomography)

The detailed examples of the 2D SEM image sections collected during FIB sectioning are shown in Figure 4 in Ref [43] and visualize osteoblast integration with the fibrous network. 3D reconstructions of cells interacting with randomly organized and aligned electrospun fibers within a 5 x 10 x 10 μm volume are presented in Figures 5 and 6 respectively. Magnified regions are shown in Figures 5(b-e) and 6(b-e) to examine interfaces between cell and fibers, and more explicitly identify the presence of filopodia that signifies efficient osteon growth. Figure 5(e) and Figure 6(e) show coherent interfaces between cells and fibers for both the aligned and random electrospun fiber orientation. Additionally, the larger 3D reconstructions for random and aligned fibers are presented in Figures 7, showing similar proliferation in 3D structure. Figure 7 also presents the cell shape within the scaffold, simplified by removing the nanofibers from the reconstruction, that allow direct indication of the degree of osteoblasts proliferation in the fiber network.

The penetration of osteoblasts within the electrospun nanofiber network can be assessed by further analysis of all 3D reconstruction, with analysis of each plane slice presented in Figure 5 in Ref [43]. Specifically, the percentage sample volume occupied by osteoblasts and electrospun PLGA fibers along the z-axis, essentially the area covered by osteoblast, filopodia or fibers in each xy section, can be found from image analysis and plotted against the z-axis coordinate distance as shown in the 3D reconstructions of Figures 5, 6, and 7. The coverage of osteoblasts within the xz plane provides further information on the distribution of cells at the random electrospun nanofiber network surface.

Variation in the volume occupied by osteoblasts at the random network surface along the y-axis of the 3D reconstructions is shown in Figure 8(a). A clear increase in the volume occupied by osteoblasts corresponds to a drop in the volume occupied by the electrospun PLGA nanofibers at the same point. This result indicates that the space filled by PLGA nanofibers constrains osteoblast volume whereas, more importantly, space not occupied by random nanofibers (i.e. voids in the nanofiber network) is filled by osteoblasts. The volume occupied by both cells and fibers varies in the y-direction and highlights fluctuations in cell coverage in the plane of the electrospun fibers. Volume occupied by cells and fibers for the aligned nanofiber network is shown in Figure 8(b), and clearly highlights considerably lower volumes occupied by cells in this aligned network when compared to the random fiber case. A more consistent cell and fiber volume is additionally observed in the aligned network, suggesting enhanced homogeneous cell coverage within aligned electrospun nanofibrous networks. Evaluation of the cell proliferation within the electrospun networks are shown along the z-direction in Figures 10(c) and (d) for random and aligned networks respectively. The random fiber network shows maximum cell volume at the surface, with decreases in the volume occupied by cells when moving further within the electrospun scaffold. Aligned networks shown a maximum volume occupied by cells at approximately 3 μm below the network surface, which then progressively decreases into the scaffold. The sum of the cell and nanofiber volume occupied, termed the sample volume, both in-plane along the y-axis and through-plane along the z-axis is summarized in Figures 10 (e) and (f) respectively. The random nanofiber networks show localized maxima both in and through-plane, indicating heterogeneities probed by the imaging technique. The aligned nanofiber network exhibits converse behavior, with homogenous sample volume distribution in both axes examined.

3.3. Confocal microscopy

Confocal microscopy was used to image the cells occupying the electrospun mats with the actin labeled as green, cell nuclei as blue and focal adhesions as red, presented in Figure 9. Focal adhesions were observed in both the random and aligned samples but differences in cell orientation and apparent focal adhesion density was found. Specifically, cells express focal adhesion markers on random fibers but with an absence of cell orientation. A greater number of focal adhesions markers were present per cell on aligned fibers networks compared to the random orientated fibers, and the cells exhibited a preferred orientation parallel to the electrospun nanofibre orientation. 3D reconstructions of cells within the nanofiber network from confocal images, as shown in Figure 10, was limited due to the relatively poor z-plane resolution of ~0.4 μm, which inhibited the direct observation of cell-nanofiber interfaces.

3.4. Gene expression

Gene expression was assessed after 4 days of culture on random fibers to identify maintenance of osteoblast phenotype and cell-nanofiber interactions. The genes studied to assess osteoblast phenotype were *IBSP, Bmp6, Bglap, Alpl* and cell-matrix interactions *Zyx, Twf,1 Lgals1, Tln1* and *Dab2.* The expression of these genes was compared to a 'housekeeping' gene *Eif4a2* (Applied Biosystems cat no. Rn0140755). Figure 6 in Ref [43] shows gene expression values for the osteoblast phenotype and demonstrates no significant differences of *Eif4a2* expression between the osteoblasts grown on plastic flask substrate when compared to the nanofiber network. The cells grown on the nanofiber network still expressed the genes that would be expected of an osteoblastic cell as shown in Table 1. However, significant differences between

gene expression for *Bmp6* and *Alpl* were found, with expression being greater in cells grown on the plastic flask. The *Bmp6* and *Alpl* gene expression results for osteoblasts on the PLGA fibers show similar values, within 10%, to cells grown in flasks. *Bmp6* codes for bone morphogenetic protein 6, a secreted protein that can induce ectopic bone formation and *Alpl* codes for alkaline phosphatase and its function is thought to participate in matrix mineralization. Additionally, increased expression was demonstrated in cells grown on flask for *Zyx*, *Lgals1* and *Dab2* genes. Zyxin, the protein product of *Zyx*, is concentrated in focal adhesion centers of the cell membrane. These adhesion centers are actin-rich structures that facilitate adhesion of the cell to the extracellular meatrix. The *Lgals1* product lectin is a galactoside-binding soluble protein and associated with cell-cell and cell-matrix adhesion. *Dab2* codes for a protein associated with reduced canonical Wnt/beta-catenin signaling pathway and is an important pathway for normal skeletogenesis [51].

4. Discussion

Electrospinning of PLGA produces networks suitable for the culture of osteoblasts as potential tissue scaffolds as shown in Figures 2-9. Both aligned and random fibers exhibit cell integration within the electrospun scaffold but critically show clear differences in such cell behavior. This variation in cell behavior must be due to the features of the network, including fiber diameter and fiber orientation. All fibers are electrospun from the same polymer solution but decreases in the average fiber diameter for the aligned organization is attributed to the centrifugal forces from the rotating drum collector causing drawing of the fibers [29, 52]. Therefore, decreases in fiber diameter as well as the spacing between fibers, clearly demonstrated in Figure 1, is occurring when aligned the electrospun fibers. Osteoblasts tend to grow along the principal fiber axis as

well as towards neighboring fibrous structures, as was indicated in previous studies [18]. Generally, cell proliferation is observable on the surface of the electrospun fiber mats but more integration of the cells below the surface of the mat occurs in random fiber samples, as shown in Figure 8, where the spacing between fibers is larger than for the aligned fiber mat. The small spacing between fibers for aligned samples limits cell proliferation and growth into the electrospun network, thus providing predominant cell growth at the top surface of the tissue scaffold. All cell growth is expected to be mediated by the presence of filopodia as imaged in Figure 5. Filopodia protrusions are presumed to be responsible for osteoblast elongation and migration into the 3D network of the electrospun nanofiber mat, thus providing coherent interfaces between cells and the electrospun nanofibers needed for an efficient bone implant [7]. We note that the electrospun networks should mimic the complexity of the natural extra cellular matrix (ECM). Our simple system is demonstrate osteoblast detection of the electrospun nanofiber direction and adherence to these fiber surfaces using filopodia, thus responding to the local nano and macroscale fibers organizations and topography. The importance of chemistry in controlling cell proliferation is removed in this paper as the same PLGA polymer is used, although previous work suggested the dominance of scaffold topography over chemistry [53]. Our studies are progressing beyond simple topography by considering high resolution 3D integration of osteoblasts within the PLGA nanofiber scaffolds. This volume fraction occupied by the electrospun fibers is similar to previous results showing a fiber volume fraction of 12% but for considerably smaller average fiber diameters (~130 nm) [44]. We therefore conclude that the porosity of electrospun nanofiber networks is potentially independent of fiber diameter and is governed more by the fiber collection process during electrospinning. Our results, with detailed filopodia imaging in 3D network of fibers at submicron level, allows analysis of cell motility as

filopodia are responsible for osteoblasts migration and adhesion to scaffolds. Although, FIB-SEM tomography is destructive technique, the connections between nanofibers and osteoblast are verified at the sub-micron filopodia level, whereas correlative confocal laser scanning microscopy was limited to larger length scale studies.

The gene expression results would suggest a less differentiated cell population growing on PLGA fibers and is consistent with microscopical observations of greater cell penetration into randomly organized substrates. In addition, the three genes *Zyx*, *Lgals1* and *Dab2* demonstrate greater expression in the cells grown on the plastic flask substrate when compared to the electrospun networks. This observation is consistent with the greater area of cell contact with the base of the plastic flask compared with cellular point contact and spanning of fibers in the PLGA samples. Specifically, the cell coverage over the plastic flask area was at least three times larger than coverage of the electrospun PLGA fiber samples used for gene expression tests. We also expect that cells contact fewer points on the PLGA sample due to porosity of the electrospun fibers, which will cause a correspond decrease in the gene expression values for the PLGA fibers when compared to the flask. However, these data indicate two salient facts; firstly, that the levels of gene expression for cells grown on PLGA fibers can be quantified. Secondly, the gene expression data demonstrates that cells grown on PLGA fibers retain an osteoblast-like phenotype. Further experiments are required to ascertain whether PLGA fibers and induced greater levels of extra cellular matrix production and mineral deposition.

5. Conclusions

Coherent interfaces between osteoblasts and electrospun PLGA tissue scaffolds were directly imaged in 3D at high spatial resolution using FIB-SEM. The presence of connections between

osteoblasts, their filopodia and the electrospun nanofibers in the tissue scaffold were observed and confirmed cell growth for demonstrable normal bone cell behavior. Control of the electrospun PLGA organization using aligned and random fiber networks produced significant changes in osteoblast growth behavior, with aligned fibers restricting cell growth to the surface of the scaffold whereas random fibers promoted integration of osteoblasts within the scaffold. The mechanism is expected to be due to increased spacing between the fibers that allowed cells to migrate into the bulk. Successful gene expression demonstrates that the osteoblast phenotype is maintained with fiber culture. This 3D imaging technique opens a new area of visualizing the cell growth on different biomaterials helping to develop and design new biomaterials for a range of clinically important applications including orthopedic. Particular examples could include osteoblast void filling of randomly aligned nanofiber networks for efficient volume packing whereas aligned nanofibers provide rapid osteoblast surface mediated growth for more superficial repair. Further studies will include optimization of porosity influencing cell infiltration and filopodia growth using human osteoblasts.

Acknowledgments

We acknowledge funding from the QMUL Pump-Priming Research Funding for Cross-Faculty Initiatives 2011-12 (EPSRC). We thank Z. Luklinska and R. J. Bailey at Queen Mary University of London NanoVision Centre for assisting with microscopy facilities.

Disclosure Statement

No competing financial interests exist for the authors U.S., T.Q., S.C.F.R., F.V.M.A., M.C. and A.H.B.

Supporting information - Data in Brief

Movies of slice and view of cells in aligned and random electrospun fibers and 3D animations of reconstructions of cells in random and aligned scaffolds, and additional figures.

This material is available free of charge via the Internet at .....

References

[1] M. Rumpler, A. Woesz, J. W. C. Dunlop, J. T. van Dongen, P. Fratzl. The effect of geometry on three-dimensional tissue growth. J R Soc Interface 5 (2008) 1173-80.

[2] J. Podporska-Carroll, J. W. Y. Ip, S. Gogolewski. Biodegradable poly(ester urethane) urea scaffolds for tissue engineering: Interaction with osteoblast-like MG-63 cells. Acta Biomater 10 (2014) 2781-91.

[3] S. Ramakrishna, K. Fujihara, W.-E. Teo, T. Yong, Z. Ma, R. Ramaseshan. Electrospun nanofibers: solving global issues. Mater Today 9 (2006) 40-50.

[4] M. M. Stevens, J. H. George. Exploring and engineering the cell surface interface. Science 310 (2005) 1135-8.

[5] K. P. Kommareddy, C. Lange, M. Rumpler, J. W. C. Dunlop, I. Manjubala, J. Cui, K. Kratz, A. Lendlein, P. Fratzl. Two stages in three-dimensional in vitro growth of tissue generated by osteoblastlike cells. Biointerphases 5 (2010) 45-52.

[6] B. Trappmann, J. E. Gautrot, J. T. Connelly, D. G. T. Strange, Y. Li, M. L. Oyen, M. A. C. Stuart, H. Boehm, B. Li, V. Vogel, J. P. Spatz, F. M. Watt, W. T. S. Huck. Extracellular-matrix tethering regulates stem-cell fate. Nat Mater 11 (2012) 642-9.

[7] K. Anselme. Osteoblast adhesion on biomaterials. Biomaterials 21 (2000) 667-81.

[8] D. Gupta, J. Venugopal, S. Mitra, V. R. G. Dev, S. Ramakrishna. Nanostructured biocomposite substrates by electrospinning and electrospraying for the mineralization of osteoblasts. Biomaterials 30 (2009) 2085-94.

[9] R. Tzezana, S. Reznik, J. Blumenthal, E. Zussman, S. Levenberg. Regulation of Stem Cell Differentiation by Control of Retinoic Acid Gradients in Hydrospun 3D Scaffold. Macromol Biosci 12 (2012) 598-607.

[10] N. F. Hughes-Brittain, L. Qiu, W. Wang, T. Peijs, C. W. M. Bastiaansen. Photoembossing of surface relief structures in polymer films for biomedical applications. J Biomed Mater Res B 102 (2012) 214-20.

[11] M. Simonet, N. Stingelin, J. G. F. Wismans, C. W. J. Oomens, A. Driessen-Mol, F. P. T. Baaijens. Tailoring the void space and mechanical properties in electrospun scaffolds towards physiological ranges. J Mat Chem B 2 (2014) 305-13.

[12] C. Vaquette, J. J. Cooper-White. Increasing electrospun scaffold pore size with tailored collectors for improved cell penetration. Acta Biomater 7 (2011) 2544-57.

[13] C. M. Murphy, F. J. O'Brien. Understanding the effect of mean pore size on cell activity in collagen-glycosaminoglycan scaffolds. Cell Adhes Migra 4 (2010) 377-81.

[14] O. Hakimi, R. Murphy, U. Stachewicz, S. Hislop, A. J. Carr. An electrospun polydioxanone patch for the localisation of biological therapies during tendon repair. Eur Cells Mater 24 (2012) 344-57.

[15] J. Xie, M. R. MacEwan, W. Z. Ray, W. Liu, D. Y. Siewe, Y. Xia. Radially Aligned, Electrospun Nanofibers as Dural Substitutes for Wound Closure and Tissue Regeneration Applications. ACS Nano 4 (2010) 5027-36.

[16] E. D. Boland, B. D. Coleman, C. P. Barnes, D. G. Simpson, G. E. Wnek, G. L. Bowlin. Electrospinning polydioxanone for biomedical applications. Acta Biomater 1 (2005) 115-23.

[17] C. Gomez-Sanchez, T. Kowalczyk, G. Ruiz De Eguino, A. Lopez-Arraiza, A. Infante, C. I. Rodriguez, T. A. Kowalewski, M. Sarrionandia, J. Aurrekoetxea. Electrospinning of poly(lactic acid)/polyhedral oligomeric silsesquioxane nanocomposites and their potential in chondrogenic tissue regeneration. J Biomater Sci Polym Ed 25 (2014) 802-25.

[18] Y. B. Truong, V. Glattauer, G. Lang, K. Hands, I. L. Kyratzis, J. A. Werkmeister, J. A. M. Ramshaw. A comparison of the effects of fibre alignment of smooth and textured fibres in electrospun membranes on fibroblast cell adhesion. Biomedical Materials 5 (2010).

[19] J. Buczynska, E. Pamula, S. Blazewicz. Mechanical Properties of (poly(L-lactide-co-glycolide))-Based Fibers Coated with Hydroxyapatite Layer. J Appl Polym Sci 121 (2011) 3702-9.

[20] M. Ngiam, S. Liao, A. J. Patil, Z. Cheng, C. K. Chan, S. Ramakrishna. The fabrication of nano-hydroxyapatite on PLGA and PLGA/collagen nanofibrous composite scaffolds and their effects in osteoblastic behavior for bone tissue engineering. Bone 45 (2009) 4-16.

[21] S. G. Kumbar, S. P. Nukavarapu, R. James, L. S. Nair, C. T. Laurencin. Electrospun poly(lactic acid-co-glycolic acid) scaffolds for skin tissue engineering. Biomaterials 29 (2008) 4100-7.

[22] M. Chen, S. Gao, M. Dong, J. Song, C. Yang, K. A. Howard, J. r. Kjems, F. Besenbacher. Chitosan/siRNA Nanoparticles Encapsulated in PLGA Nanofibers for siRNA Delivery. ACS Nano 6 (2012) 4835-44.

[23] K. Kim, M. Yu, X. H. Zong, J. Chiu, D. F. Fang, Y. S. Seo, B. S. Hsiao, B. Chu, M. Hadjiargyrou. Control of degradation rate and hydrophilicity in electrospun non-woven poly(D,L-lactide) nanofiber scaffolds for biomedical applications. Biomaterials 24 (2003) 4977-85.

[24] X. Xin, M. Hussain, J. J. Mao. Continuing differentiation of human mesenchymal stem cells and induced chondrogenic and osteogenic lineages in electrospun PLGA nanofiber scaffold. Biomaterials 28 (2007) 316-25.

[25] Y. Liu, M. H. Rafailovich, R. Malal, D. Cohn, D. Chidambaram. Engineering of bio-hybrid materials by electrospinning polymer-microbe fibers. P Natl Acad Sci USA 106 (2009) 14201-6.

[26] Y. B. Truong, V. Glattauer, K. L. Briggs, S. Zappe, J. A. M. Ramshaw. Collagen-based layer-by-layer coating on electrospun polymer scaffolds. Biomaterials 33 (2012) 9198-204.

[27] D. Li, Y. N. Xia. Electrospinning of nanofibers: Reinventing the wheel? Adv Mater 16 (2004) 1151-70.

[28] G. C. Rutledge, S. V. Fridrikh. Formation of fibers by electrospinning. Adv Drug Deliver Rev 59 (2007) 1384-91.

[29] P. Kiselev, J. Rosell-Llompart. Highly aligned electrospun nanofibers by elimination of the whipping motion. J Appl Polym Sci 125 (2012) 2433-41.

[30] S. Megelski, J. S. Stephens, D. B. Chase, J. F. Rabolt. Micro- and Nanostructured Surface Morphology on Electrospun Polymer Fibers. Macromolecules 35 (2002) 8456-66.

[31] A. Arinstein, M. Burman, O. Gendelman, E. Zussman. Effect of supramolecular structure on polymer nanofibre elasticity. Nat Nanotechnol 2 (2007) 59-62.

[32] E. García-Gareta, M. J. Coathup, G. W. Blunn. Osteoinduction of bone grafting materials for bone repair and regeneration. Bone 81 (2015) 112-21.

[33] P. K. Mattila, P. Lappalainen. Filopodia: molecular architecture and cellular functions. Nat Rev Mol Cell Bio 9 (2008) 446-54.

[34] F. Xue, D. M. Janzen, D. A. Knecht. Contribution of Filopodia to Cell Migration: A Mechanical Link between Protrusion and Contraction. Inter J Cell Bio 2010 (2010) 507821.

[35] L. E. Smith, R. Smallwood, S. Macneil. A Comparison of Imaging Methodologies for 3D Tissue Engineering. Microscopy Research and Technique 73 (2010) 1123-33.

[36] J.-W. Lee, K.-B. Lee, H.-S. Jeon, H.-K. Park. Effects of Surface Nano-Topography on Human Osteoblast Filopodia. Anal Sci 27 (2011) 369-74.

[37] E. Martinez, E. Engel, C. Lopez-Iglesias, C. A. Mills, J. A. Planell, J. Samitier. Focused ion beam/scanning electron microscopy characterization of cell behavior on polymer micro-/nanopatterned substrates: A study of cell-substrate interactions. Micron 39 (2008) 111-6.

[38] J. R. Wilson, W. Kobsiriphat, R. Mendoza, H. Y. Chen, J. M. Hiller, D. J. Miller, K. Thornton, P. W. Voorhees, S. B. Adler, S. A. Barnett. Three-dimensional reconstruction of a solid-oxide fuel-cell anode. Nat Mater 5 (2006) 541-4.

[39] J. S. Earl, R. K. Leary, J. S. Perrin, R. Brydson, J. P. Harrington, K. Markowitz, S. J. Milne. Characterization of dentine structure in three dimensions using FIB-SEM. J Microsc 240 (2010) 1-5.

[40] M. Zietara, A. Kruk, A. Gruszczynski, A. Czyrska-Filemonowicz. FIB-SEM tomography of 4th generation PWA 1497 superalloy. Materials Characterization 87 (2014) 143-8.

[41] D. A. M. De Winter, C. T. W. M. Schneijdenberg, M. N. Lebbink, B. Lich, A. J. Verkleij, M. R. Drury, B. M. Humbel. Tomography of insulating biological and geological materials using focused ion beam (FIB) sectioning and low-kV BSE imaging. J Microsc 233 (2009) 372-83.

[42] A. Friedmann, A. Cismak, C. Tautorat, P. J. Koester, W. Baumann, J. Held, J. Gaspar, P. Ruther, O. Paul, A. Heilmann. FIB preparation and SEM investigations for three-dimensional analysis of cell cultures on microneedle arrays. Scanning 33 (2011) 1-9.

[43] U. Stachewicz, T. Qiao, S. C. F. Rawlinson, F. Viga De Macedo Almeida, W. Q. Li, M. Catell, A. H. Barber. Data in support to 3D imaging of cell interactions with electrospun nanofiber membranes Data in Brief submitted (2015).

[44] U. Stachewicz, F. Modaresifar, R. J. Bailey, T. Peijs, A. H. Barber. Manufacture of Void-Free Electrospun Polymer Nanofiber Composites with Optimized Mechanical Properties. ACS Appl Mater Interfaces 4 (2012) 2577–82.

[45] A. J. Bushby, K. M. Y. P'ng, R. D. Young, C. Pinali, C. Knupp, A. J. Quantock. Imaging three-dimensional tissue architectures by focused ion beam scanning electron microscopy. Nat Protoc 6 (2011) 845-58.

[46] R. J. Bailey, R. Geurts, D. J. Stokes, F. de Jong, A. H. Barber. Evaluating focused ion beam induced damage in soft materials. Micron 50 (2013) 51-6.

[47] U. Stachewicz, R. J. Bailey, H. Zhang, C. A. Stone, C. R. Willis, A. H. Barber. Wetting Hierarchy in Oleophobic 3D Electrospun Nanofiber Networks. ACS Appl Mater Interfaces in press (2015) DOI: 10.1021/acsami.5b04272.

[48] S. C. F. Rawlinson, I. J. McKay, M. Ghuman, C. Wellmann, P. Ryan, S. Prajaneh, G. Zaman, F. J. Hughes, V. J. Kingsmill. Adult Rat Bones Maintain Distinct Regionalized Expression of Markers Associated with Their Development. PloS one 4 (2009).

[49] J. Z. Li, H. W. Li, G. R. Hankins, A. S. Lieu, E. Noh, L. Jacobson, D. D. Pittman, J. A. Chiorini, G. A. Helm. Different osteogenic potentials of recombinant human BMP-6 adeno-associated virus and adenovirus in two rat strains. Tissue Engineering 12 (2006) 209-19.

[50] A. C. Akman, R. S. Tigli, M. Gumusderelioglu, R. M. Nohutcu. Bone Morphogenetic Protein-6-loaded Chitosan Scaffolds Enhance the Osteoblastic Characteristics of MC3T3-E1 Cells. Artificial Organs 34 (2010) 65-74.

[51] Y. Wang, Y.-P. Li, C. Paulson, J.-Z. Shao, X. Zhang, M. Wu, W. Chen. Wnt and the Wnt signaling pathway in bone development and disease. Frontiers in Bioscience-Landmark 19 (2014) 379-407.

[52] J. Xie, M. R. MacEwan, X. Li, S. E. Sakiyama-Elbert, Y. Xia. Neurite Outgrowth on Nanofiber Scaffolds with Different Orders, Structures, and Surface Properties. ACS Nano 3 (2009) 1151-9.

[53] T. Sun, D. Norton, R. J. McKean, J. W. Haycock, A. J. Ryan, S. MacNeil. Development of a 3D cell culture system for investigating cell interactions with electrospun fibers. Biotechnology and Bioengineering 97 (2007) 1318-28.

Figure legends

Figure 1. Scanning electron micrographs of electrospun PLGA fibers deposited (a) randomly (b) aligned and (c) fiber diameter distribution histogram for random and aligned fibers.

Figure 2. Scanning electron micrographs of electrospun PLGA fibers incorporating osteoblasts (UMR106) showing (a) cell spreading over the fibrous network and (b) integration of osteoblasts and filopodia within the fibrous network. Filipodia are indicated with arrows.

Figure 3. Scanning electron micrographs of electrospun PLGA fibers with osteoblasts showing (a) cell (UMR106) spreading over the random fibrous network (b) integration of osteoblasts (UMR106) and filopodia within the random fibrous network (c) cell (MC3T3-E1) elongation in the direction of aligned fibers and (d) integration of osteoblasts (MC3T3-E1) and filopodia within the aligned fibrous network. Cells are indicated with arrows.

Figure 4. Scanning electron micrographs of (a) cross-sections of random electrospun PLGA fiber networks showing filopodia formation on fibers with osteoblast (UMR106) integration within the fibrous mat (b) close up of filopodia created between the random fibers (c) filopodia formation from osteoblast-like MC3T3-E1 within an aligned electrospun fiber network and (d) close up of filopodia formation between aligned fibers. Filopodia are indicated with arrows.

Figure 5. 3D reconstructions of osteoblasts (UMR106) (in green) growing within a random electrospun PLGA nanofiber network (in red) showing (a) volume reconstruction with dimensions of 20×5×10 μm, indicating two regions of interest with (b) volume reconstruction of region A and (c) 3D reconstruction of osteoblasts only showing the advancing cells in region A,

and (d) volume reconstruction of region B and (e) volume rotation of the 3D reconstruction of region B highlighting coherent nanofiber-cell interfaces. See videos 6 in Ref [43].

Figure 6. 3D reconstructions of osteoblasts-like MC3T3-E1 (in green) growing within an aligned electrospun PLGA nanofiber network (in red) showing (a) volume reconstruction with dimensions of 20×5×10 μm, indicating two regions of interest with (b) volume reconstruction of region A and (c) 3D reconstruction of osteoblasts only showing the advancing cells in region A and (d) volume reconstruction of region B and (e) volume rotation of the 3D reconstruction of region B highlighting coherent nanofiber-cell interfaces. See videos 2 in Ref [43].

Figure 7. Larger 3D reconstruction (volume of 30 × 28 × 22 μm) of osteoblasts (in green) growing into (a) random electrospun PLGA nanofiber networks (in red), (b) osteoblasts (MC3T3-E1) reconstruction only without the nanofiber scaffold and (c) 3D reconstruction (volume 50 × 28 × 6 μm) of osteoblasts growing within an aligned electrospun PLGA nanofiber network, with (d) the osteoblasts (MC3T3-E1) reconstruction with the aligned nanofiber scaffold removed. See videos 4 and 8 in Ref [43].

Figure 8. Osteoblast and fiber volume occupied as a function of distance along the y-axis of the 3D reconstructed sample in (a) the random electrospun PLGA fiber network volume and (b) for aligned electrospun PLGA fiber network. Sample volume occupied as a function of z-axis depth for the 3D network for (c) osteoblasts and random electrospun PLGA nanofibers and (d) osteoblasts and aligned electrospun PLGA nanofibers. Sample volume occupied by osteoblasts in electrospun PLGA nanofibers randomly oriented and aligned as a function of (e) xy-plane and (f) z-axis depth, for the 'sliced and view' of large volume samples presented in Figure 7.

Figure 9. Confocal microscopy images of osteoblasts (MC3T3-E1) cultured on PLGA fibers for 4 days. The actin (green), nuclei (blue) and red (focal adhesions) demonstrate an extensive cytoskeletal network and numerous focal adhesions, with poorly organized cell distribution in (a) and (b) for random fibers; (c) and (d) for aligned fibers demonstrate more focal adhesion sites and parallel elongated alignment of the cells. Scale bar is 50 μm.

Figure 10. Projected z-stack of optical confocal images of osteoblasts cultured for 4 days on random and aligned PLGA electrospun fibers. (a) shows the xy plane orientation for osteoblasts (MC3T3-E1) cultured on random fiber networks and (b) shows xy plane orientation for osteoblasts (MC3T3-E1) cultured on aligned fiber networks. (c) and (d) show zx plane orientation for random and aligned networks respectively, highlighting cell integration within the nanofiber scaffolds.

Figure 1.

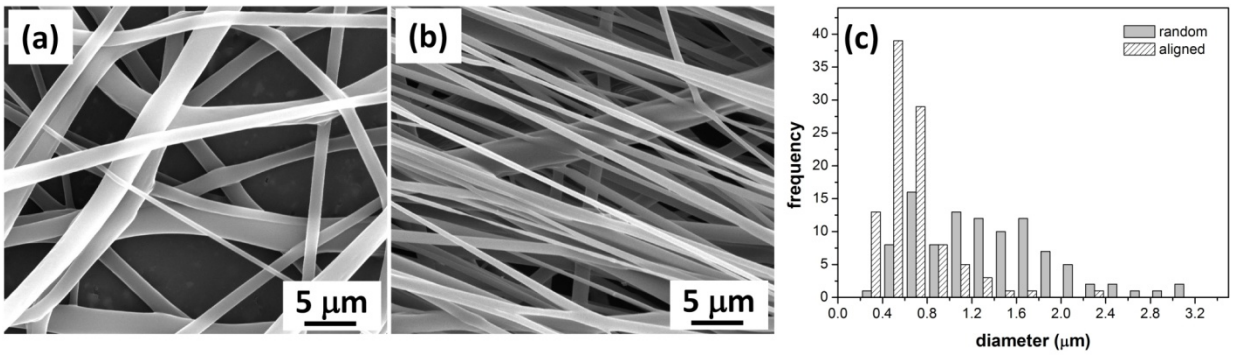

Figure 2.

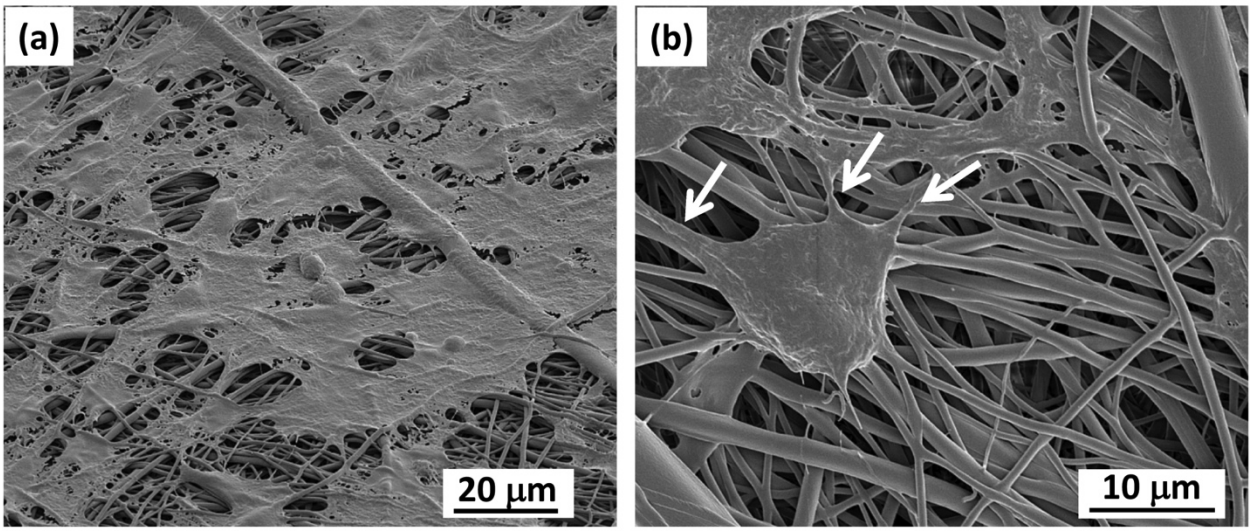

Figure 3.

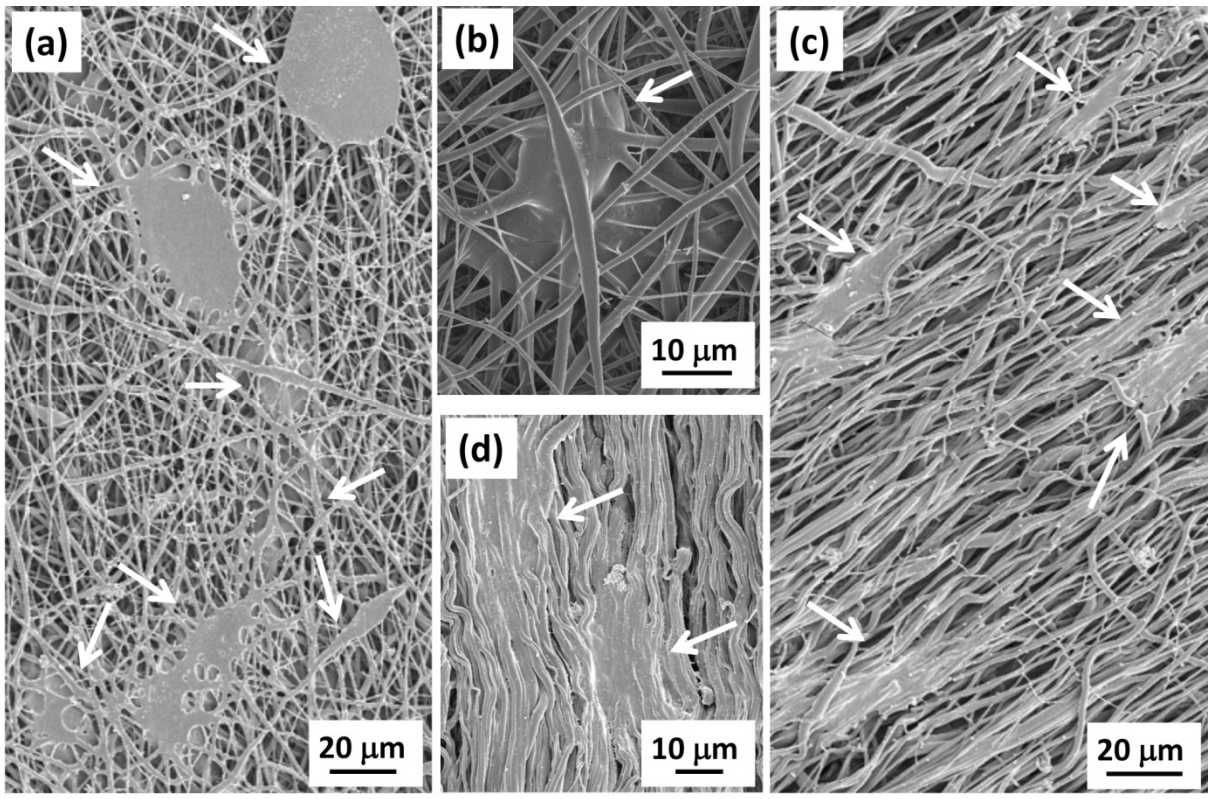

Figure 4.

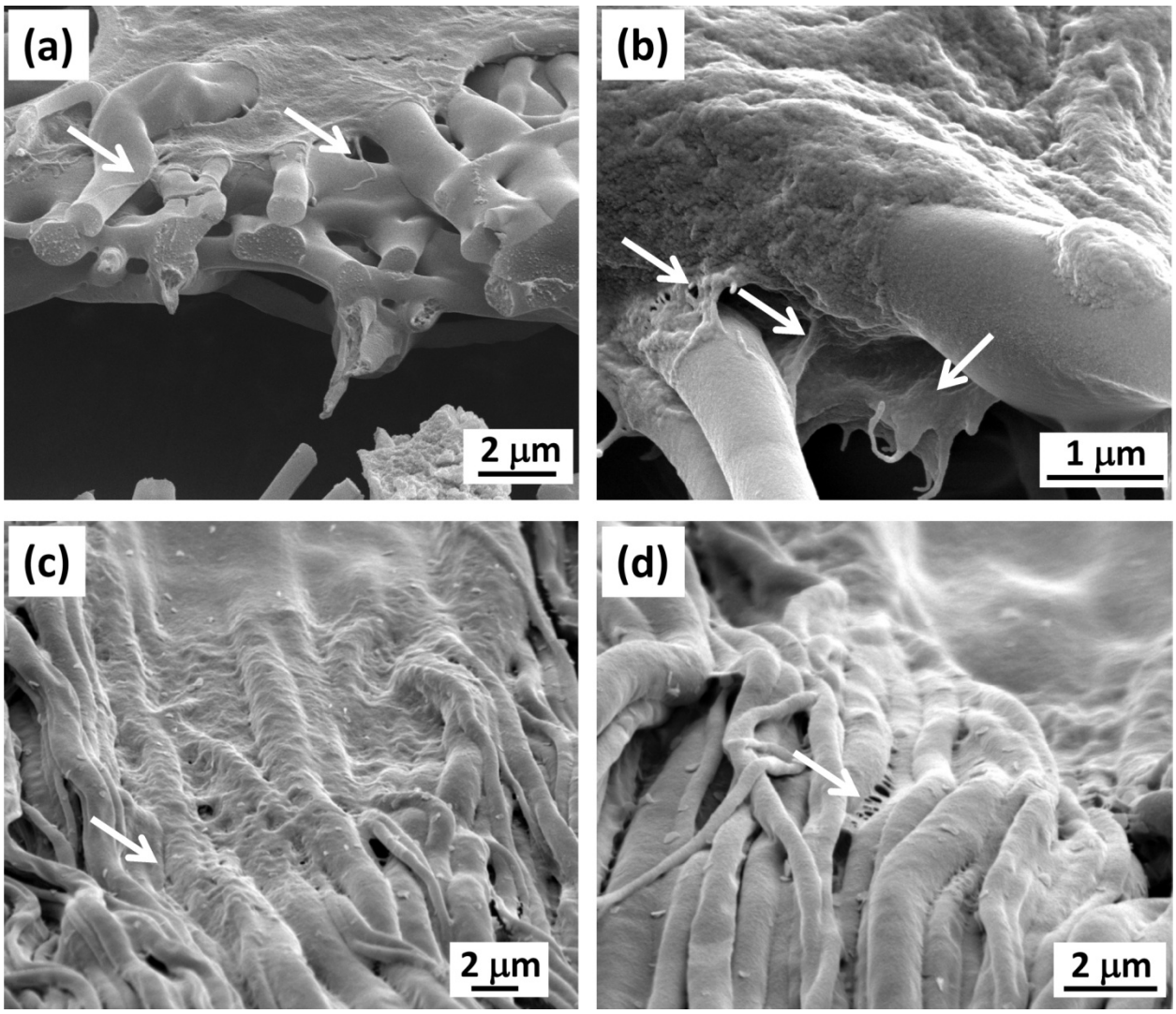
(a)
2 μm
(b)
1 μm
(c)
2 μm
(d)
2 μm

Figure 5.

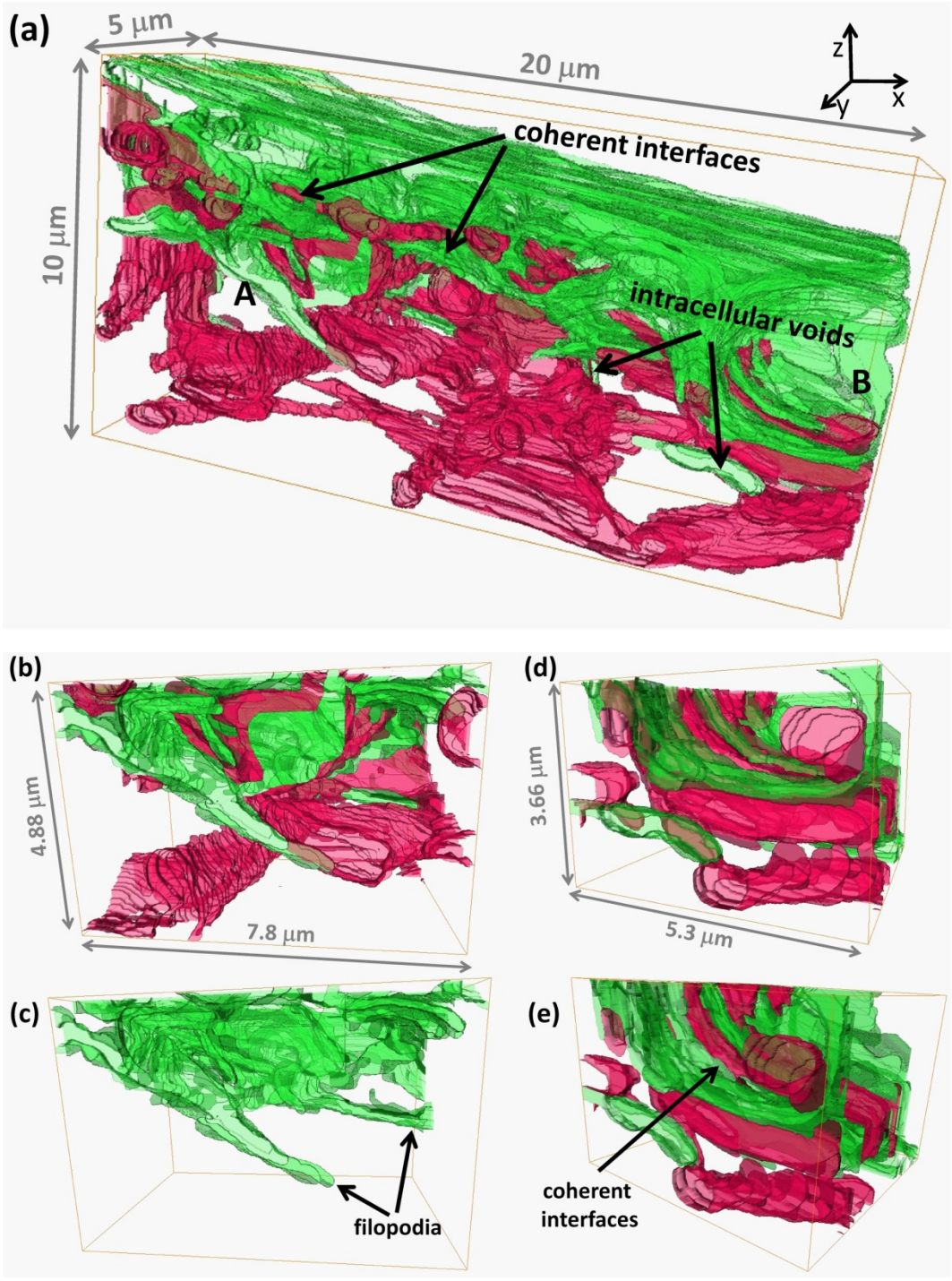
(a)
5 μm
20 μm
z
y
x
coherent interfaces
10 μm
A
intracellular voids
B
(b)
4.88 μm
7.8 μm
(d)
3.66 μm
5.3 μm
(c)
filopodia
(e)
coherent
interfaces

Figure 6.

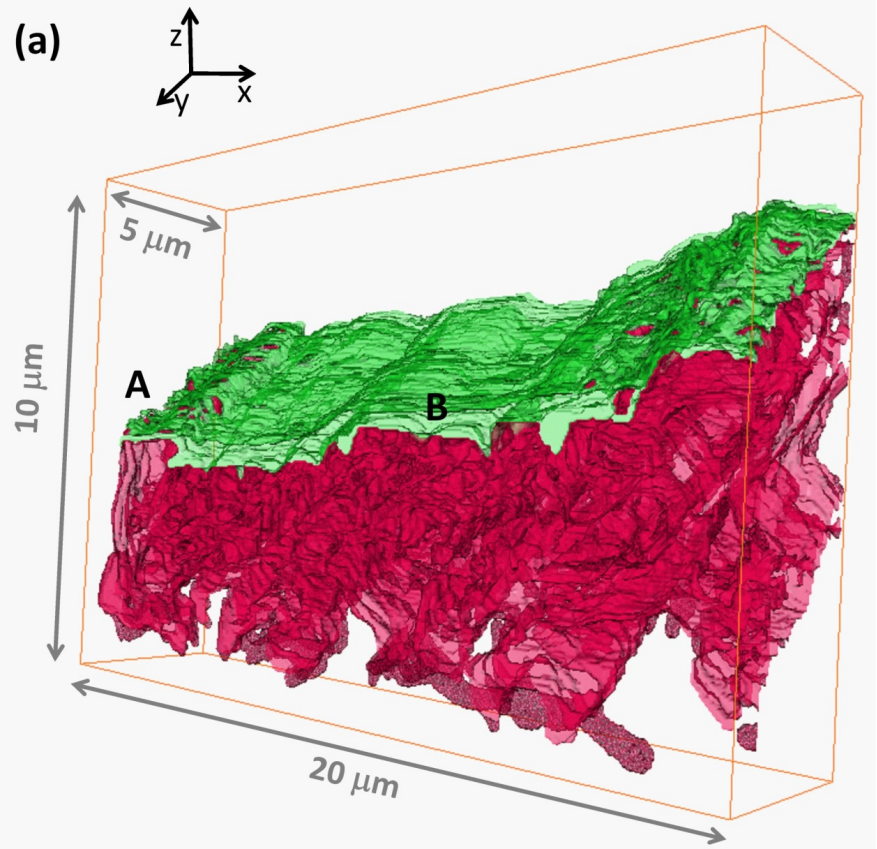

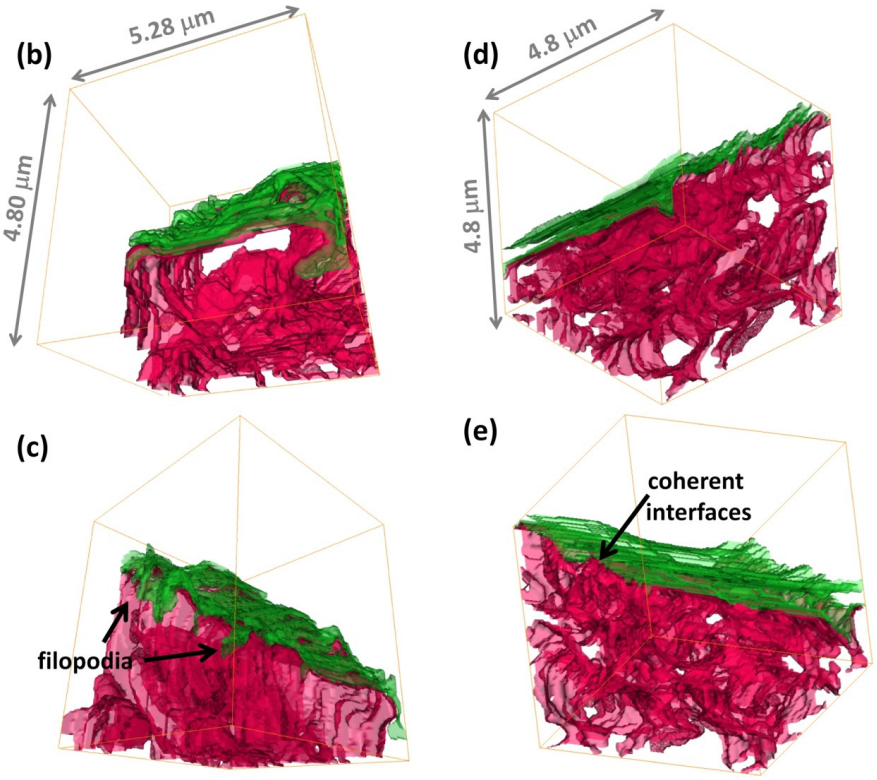
(b)
5.28 μm
4.80 μm
(d)
4.8 μm
4.8 μm
(c)
filopodia
(e)
coherent
interfaces

Figure 7.

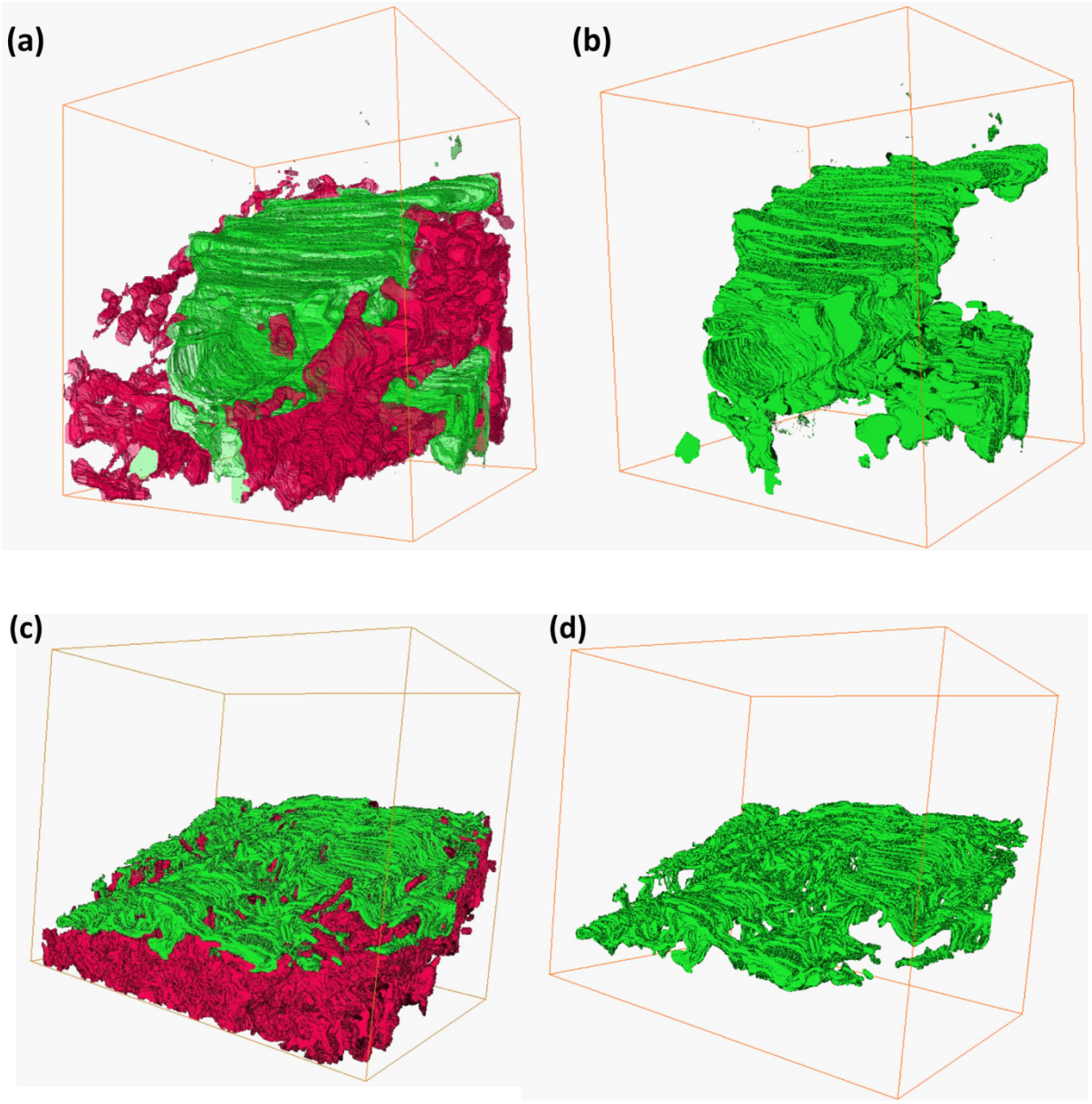

Figure 8.

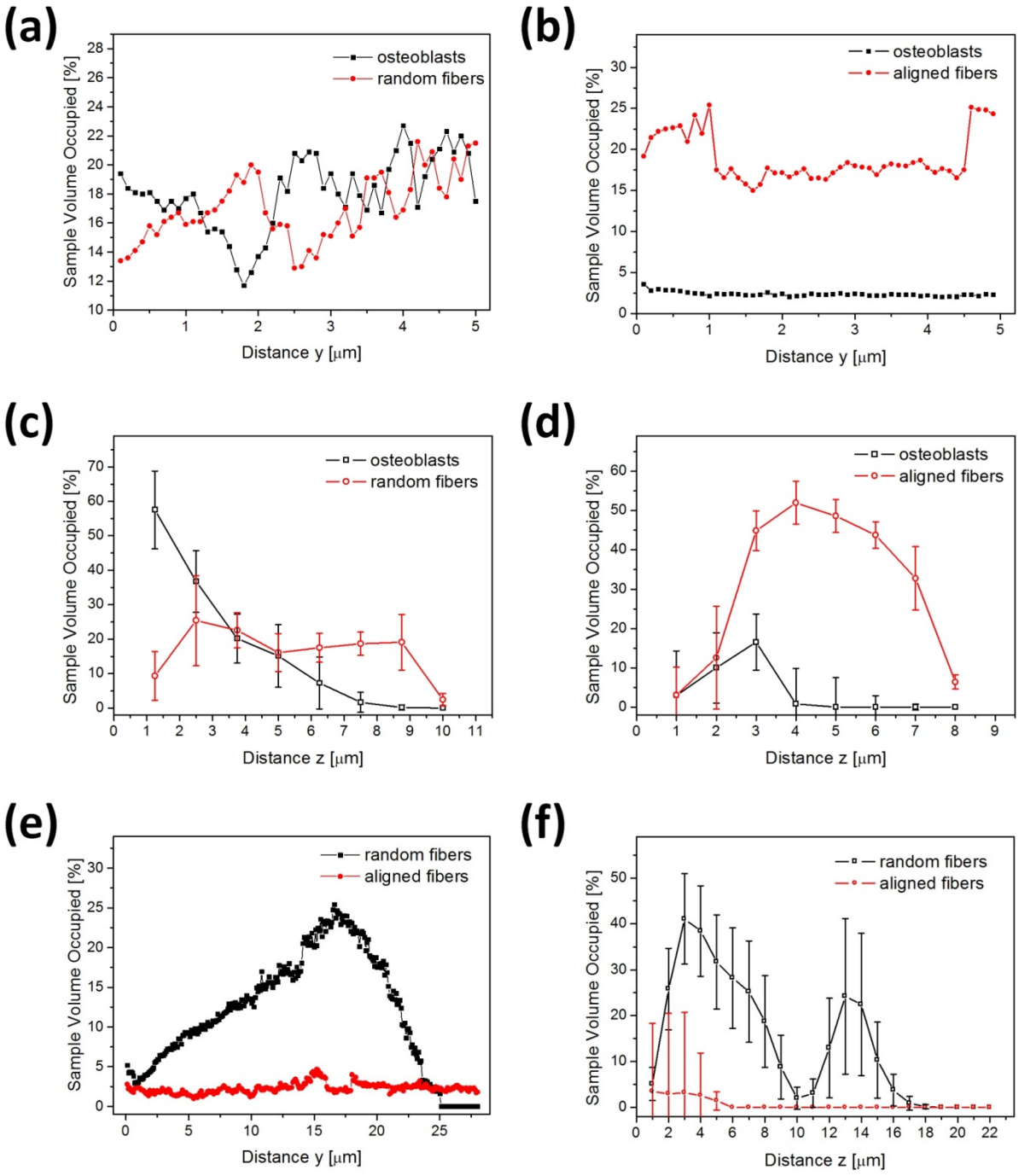
(a)
osteoblasts
random fibers
Sample Volume Occupied [%]
Distance y [μm]
(b)
osteoblasts
aligned fibers
Sample Volume Occupied [%]
Distance y [μm]
(c)
osteoblasts
random fibers
Sample Volume Occupied [%]
Distance z [μm]
(d)
osteoblasts
aligned fibers
Sample Volume Occupied [%]
Distance z [μm]
(e)
random fibers
aligned fibers
Sample Volume Occupied [%]
Distance y [μm]
(f)
random fibers
aligned fibers
Sample Volume Occupied [%]
Distance z [μm]

Figure 9.

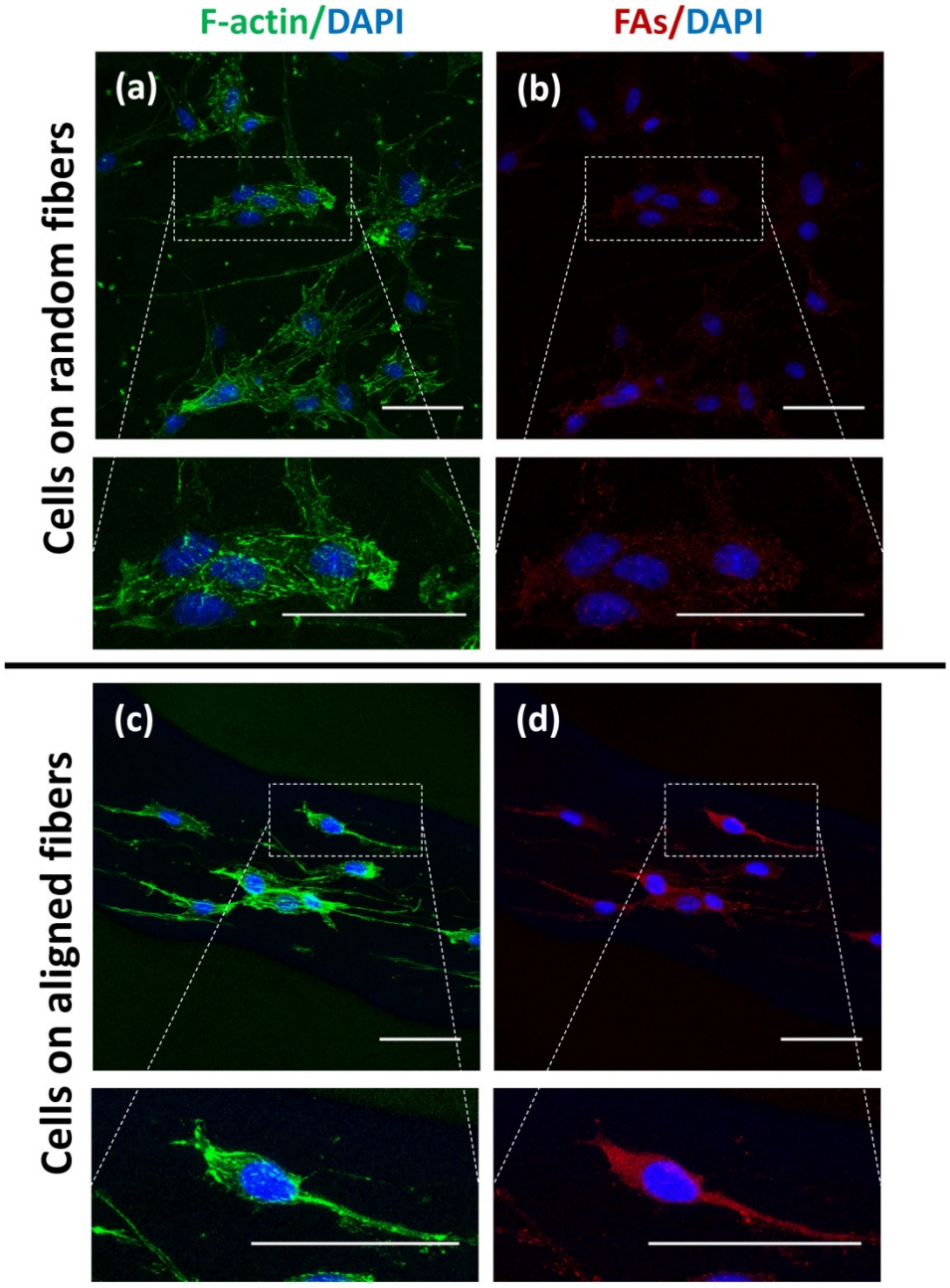
F-actin/DAPI
FAs/DAPI
(a)
(b)
Cells on random fibers
(c)
(d)
Cells on aligned fibers

Figure 10.